Applied Microscopy
Korean Society of Microscopy

pISSN 2287-5123 · eISSN 2287-4445
http://dx.doi.org/10.9729/AM.2012.42.3.151

Transmission Electron Microscopy Study of Stacking Fault Pyramids Formed in Multiple Oxygen Implanted Silicon-on-Insulator Material

Ju-cheol Park*, June-dong Lee[1], Steve J. Krause[1]

Center for Materials Analysis, Research Institute for Advanced Materials, Seoul National University, Seoul 151-742, Korea
[1]Department of Chemical, Bio and Materials Engineering, Arizona State University, Tempe, Arizona 85287, USA

*Correspondence to:
Park JC,
Tel: +82-2-880-5746
Fax: +82-2-871-9095
E-mail: jucheolpark@snu.ac.kr

Received August 22, 2012
Revised September 6, 2012
Accepted September 7, 2012

The microstructure of various shapes of stacking fault pyramids (SFPs) formed in multiple implant/anneal Separation by Implanted Oxygen (SIMOX) material were investigated by plan-view and cross-sectional transmission electron microscopy. In the multiple implant/anneal SIMOX, the defects in the top silicon layer are confined at the interface of the buried oxide layer at a density of ~10^6 cm^{-2}. The dominant defects are perfect and imperfect SFPs. The perfect SFPs were formed by the expansion and interaction of four dissociated dislocations on the {111} pyramidal planes. The imperfect SFPs show various shapes of SFPs, including I-, L-, and Y-shapes. The shape of imperfect SFPs may depend on the number of dissociated dislocations bounded to the top of the pyramid and the interaction of Shockley partial dislocations at each edge of {111} pyramidal planes.

Key Words: SIMOX, SOI, Defects, Stacking fault pyramids, TEM

INTRODUCTION

Separation-by-Implantation-of-Oxygen (SIMOX) process has been a well-established fabrication technology of silicon-on-insulator (SOI) material for complementary metal-oxide-semiconductor (CMOS) circuits with increased radiation hardness and higher operating speed (Sears et al., 2006). However, high density (~10^8 cm^{-2}) of through-thickness dislocations (TTD) in the top Si layer of SIMOX is one of the most serious problems. Several groups reported methods to remarkably reduce TTD densities to <10^5 cm^{-2} (Hill et al., 1988; van Ommen, 1988; El-Ghor et al., 1990). One of the typical methods is multiple low dose implants with sequential high-temperature anneals (Cheek & Chen, 1988; Margail et al., 1989; Park et al., 1992; Venables et al., 1992). In the multiple implant/anneal SIMOX material, the dominant defects are ~10^6 cm^{-2} of stacking fault pyramids (SFPs) and residual oxide precipitates pinning dissociated dislocations (Park et al., 1992). These defects are confined to the buried oxide interface but still degrade the quality of the top silicon layer. To improve the quality of the layer, the formation mechanism of the defects should be understood. Crean et al. (1992) have argued that SFPs are formed at the Si/SiO_2 interface as part of the regrowth mechanisms of the top silicon layer during high temperature annealing and the dissolution of SiO_2 precipitates. However, we found many imperfect SFPs which could not be formed as the regrowth of Si layer. There has been no systematic study to understand the formation of imperfect SFPs in multiple implant/anneal material. Therefore, to understand the formation mechanism of various SFPs, Burgers vectors of dissociated dislocations pinned to the residual precipitates were determined by the transmission electron microscopy (TEM) bright field (BF) and weak beam dark field (WBDF) imaging technique with tilting experiments. The nature of stacking faults in SFPs was investigated by high-resolution electron microscopy.

In this paper, we studied a qualitative model for the formation mechanism of imperfect SFPs in SIMOX material. It will

be shown that the shape of imperfect SFPs mainly depends on the number of four narrow stacking faults (NSFs) and the configuration of various Burgers vectors of Shockley partial dislocations bounded to a residual oxide precipitate. This mechanism will provide better understanding for the formation and evolution of defects, and contribute to further reduction of the critical defects in the top silicon layer.

MATERIALS AND METHODS

Silicon (100) wafers were sequentially triple implanted to doses of $6/6/6\times10^{17}$ or $5/5/8\times10^{17}$ cm^{-2} at 200 keV and 620°C. After each implantation the wafers were at 950°C or 1,000°C for 2 hours and annealed at 1,325°C for 4 hours in argon ambient plus 5% oxygen. The effect of intermediate temperature annealing was investigated by annealing wafers after the third and final implant at temperatures from 800°C to 1,350°C in 50°C increments for 2 hours in and Ar/0.5% O_2 ambient. Cross-section (XTEM) and plan view (PTEM) transmission electron microscopy specimens were examined using a conventional BF and WBDF techniques in JEOL 2000FX (Tokyo, Japan) operating at 200 keV. Burgers vector and true directions of dislocations were determined by diffraction contrast analysis using WBDF and by trace analysis using BF, respectively.

RESULTS AND DISCUSSION

Formation of Perfect SFPs

Cross-sectional and plan-view TEM observations at each stage of the multiple implant/anneal cycles at 1,250~1,325°C show that in each case, residual precipitates pinning from one to four dislocations survive the annealing process and are located just above the buried oxide and residual defects. The length of the dislocations is limited by the relative location of the precipitates in the top silicon layer on which they terminate at the upper interface of the buried oxide (Fig. 1). PTEM observations of the samples annealed at 1,250°C showed that

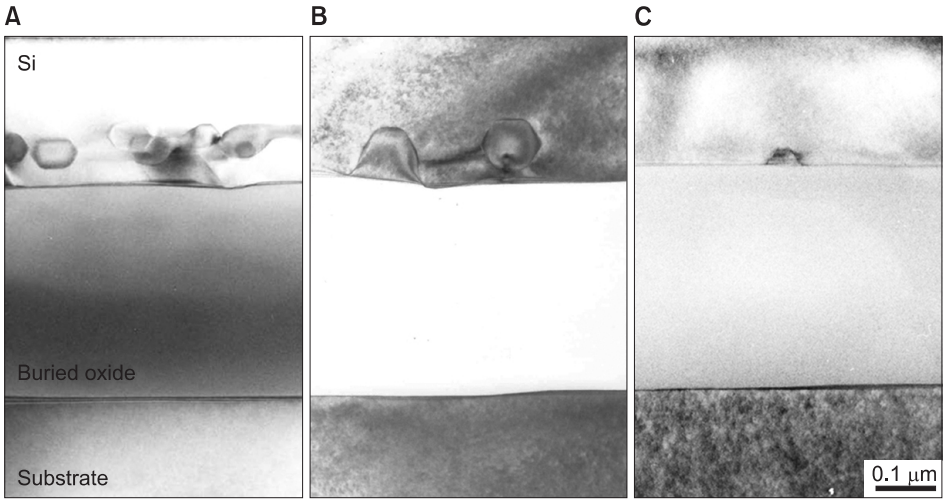

Fig. 1. Cross-sectional transmission electron microscopy micrographs of the samples third-annealed at (A) 1,250°C, (B) 1,300°C, and (C) 1,325°C.

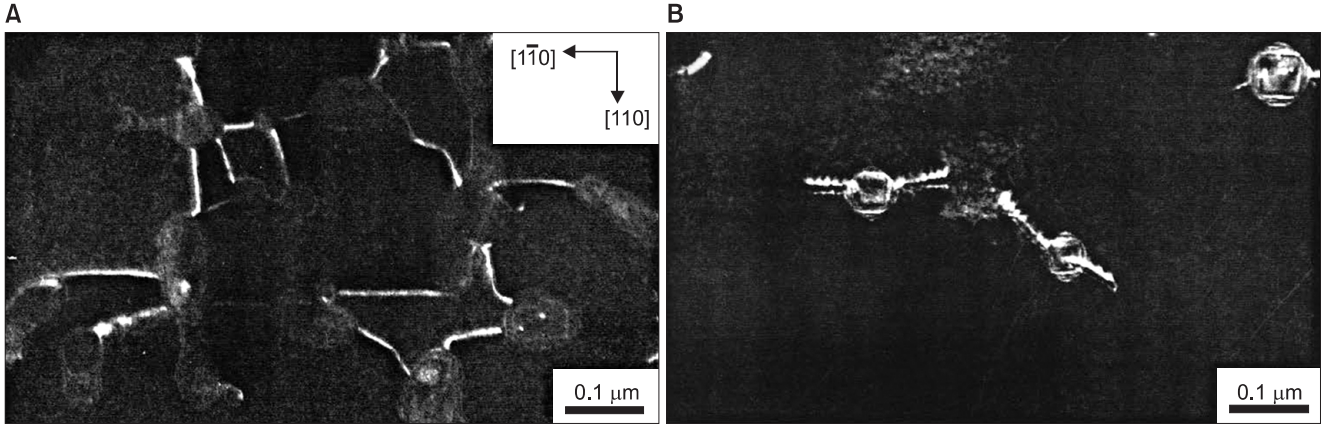

Fig. 2. Plan-view TEM micrographs of the samples third-annealed at (A) 1,250°C and (B) 1,325°C.

the precipitates form an almost orthogonal grid of precipitates network elongated along <110> directions connected numerous dislocations (Fig. 2A). During high temperature annealing at 1,325°C the precipitates are considerably dissolved and result in isolated residual precipitates pinning dislocations which are called as precipitate-dislocation complexes (PDCs) shown in Fig. 2B. WBDF analysis shows that the dislocations pinned to the precipitates were dissociated into two partial dislocations, which are called as NSFs.

PTEM observations of the samples at each stage of the multiple implant/anneal cycles at 1,325°C show that the distance between the residual precipitates and the buried oxide (and thus also the length of the NSFs) decreases with each implant/anneal cycle from an average of 115 nm after the first cycle to about 100 nm after the second cycle and finally to about 65 nm after the third implant/anneal cycle (Fig. 3). After the complete third anneal, SFPs are predominantly found (Fig. 3D). From the results, we found that the transformation from a collection of NSFs to a SFP is closely related to the degree of completeness of annealing and the length of the NSFs. This, we calculated the total energy associated with each defect configuration to evaluate a critical length of the transformation (Lee et al., 1993). The total energy has two contributions: 1) the energy of the stacking fault that is proportional to the fault area and is therefore larger for SFPs, and 2) the strain energy of the bounding dislocations that is related to the Burgers vector and length of the dislocations and is therefore larger for the four NSFs. The results of the calculation indicate that it is energetically favorable for a collection of four NSFs to transform to a SFP below 620 Å of a critical projected length.

We investigated the characteristics of SFP by using various TEM techniques. Trace analysis using bright-field methods indicate that the fully formed defects consist of a perfect pyramid of stacking faults on the four {111} pyramidal planes, and the base of the pyramid is the upper interface of the buried oxide. Diffraction contrast analysis shows that the total dislocations with 1/2<110> Burgers vectors are dissociated with a separation of 50 to 90 Å into two Shockley partial dislocations bounding NSFs and that expanded stacking faults consist of two Shockley partials bounding two stacking faults on the intersecting planes and one stair-rod dislocation

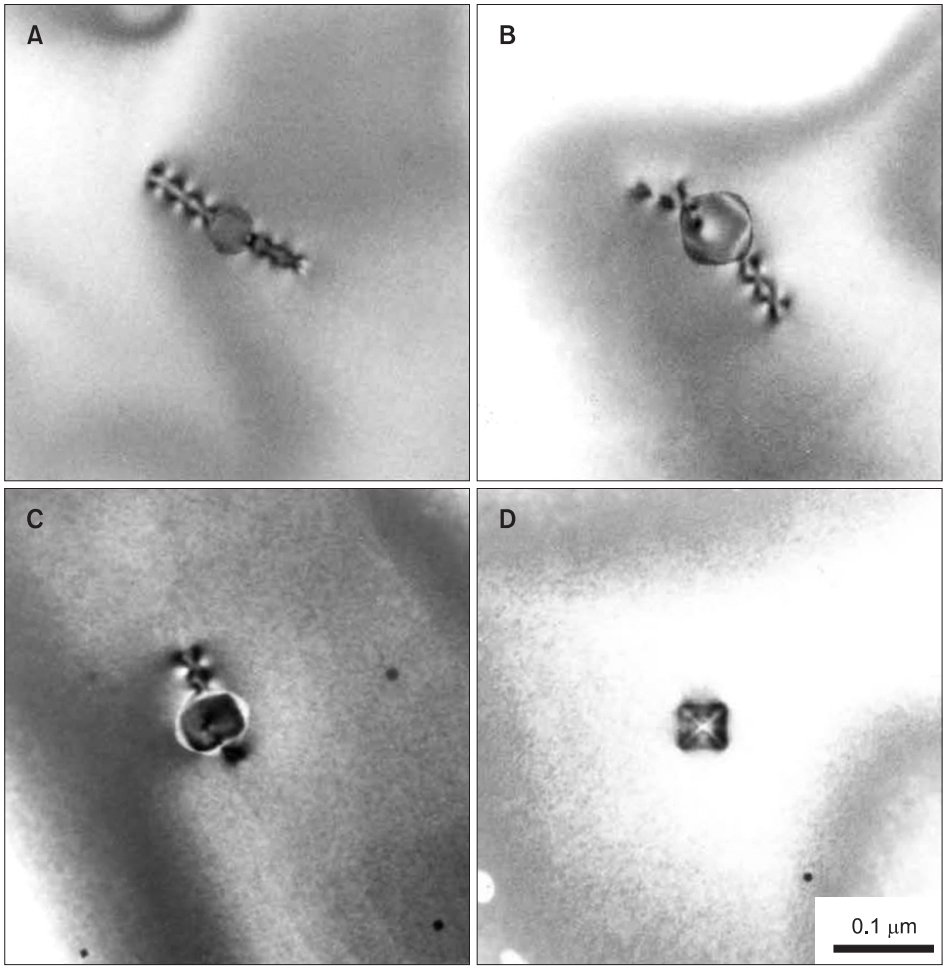

Fig. 3. Plan-view TEM micrographs of precipitate-dislocation complexes found in the samples annealed at 1,325°C. (A) First-annealed, (B) second-annealed, (C) third-incomplete annealed, and (D) third-complete annealed. Note that the length of dislocations decreases after each additional implant and anneal.

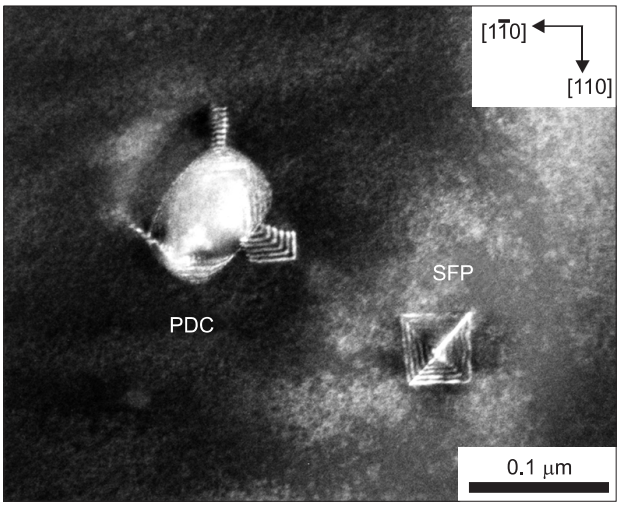

Fig. 4. Weak-beam dark field micrograph showing a precipitate-dislocation complex (PDC) and a stacking fault pyramid (SFP) in the sample in complete-annealed at 1,325°C.

at the edge of two planes (Fig. 4). These observations indicate that when two Shockley partial dislocations bounding NSFs intersect on adjacent planes, they form one stair-rod dislocation at the edge, and the NSFs are expanded. Thus, it can be suggested that if a residual precipitate holds four NSFs on each {111} pyramidal plane and the NSFs could touch each other on the precipitate, then a pyramid of stacking faults and stair-rod dislocations can be developed from the joined point of the NSFs. The schematic diagrams illustrating this procedure are shown in Fig. 5. As a result, the formation of a perfect SFP requires four NSFs with a critical length of <620 Å.

Formation of Imperfect SFPs

In addition to perfect SFPs, various shapes of imperfect SFPs, where at least one edge of the pyramid has not been completely formed, were more frequently found in the multiple implant/anneal SIMOX. However, in spite of knowing the formation mechanism of SFPs, it is still in

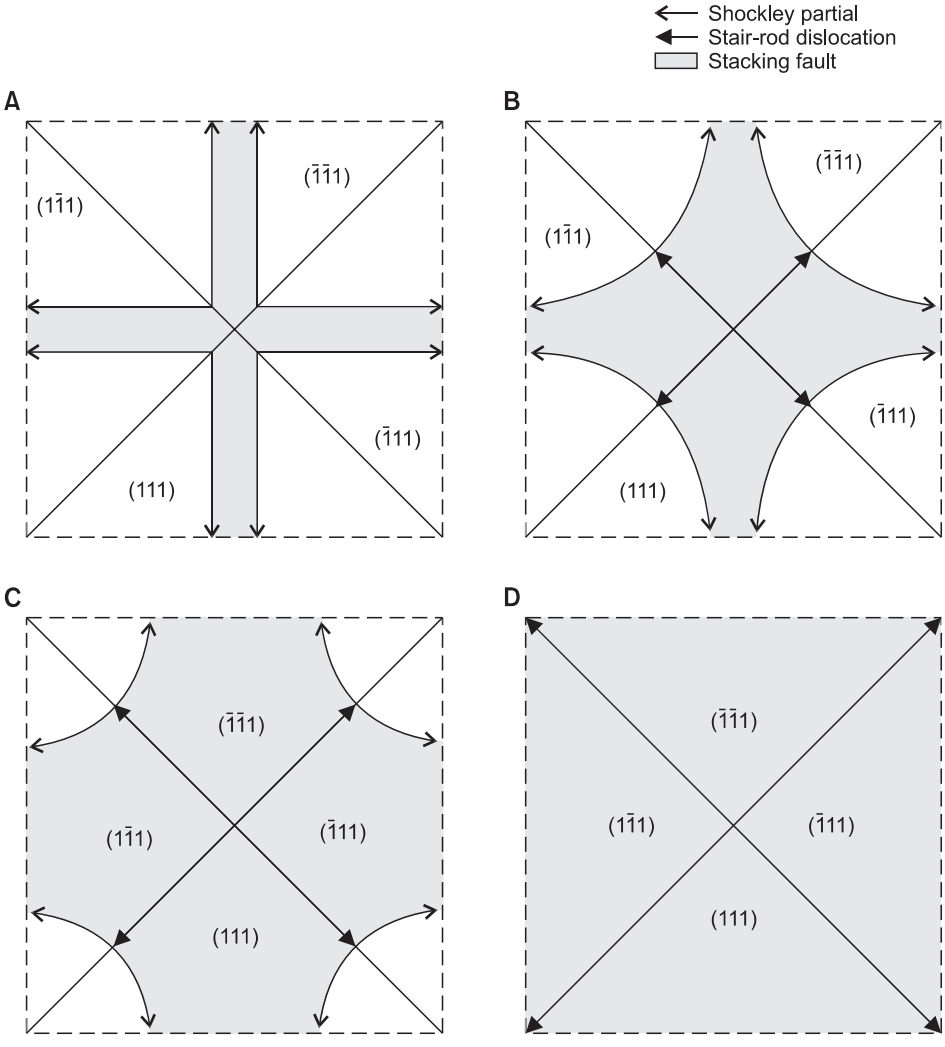

Fig. 5. Schematic diagrams showing the transformation from four narrow stacking faults to a stacking fault pyramid. Note that stair-rod dislocations were formed from the top of the pyramid at its edge.

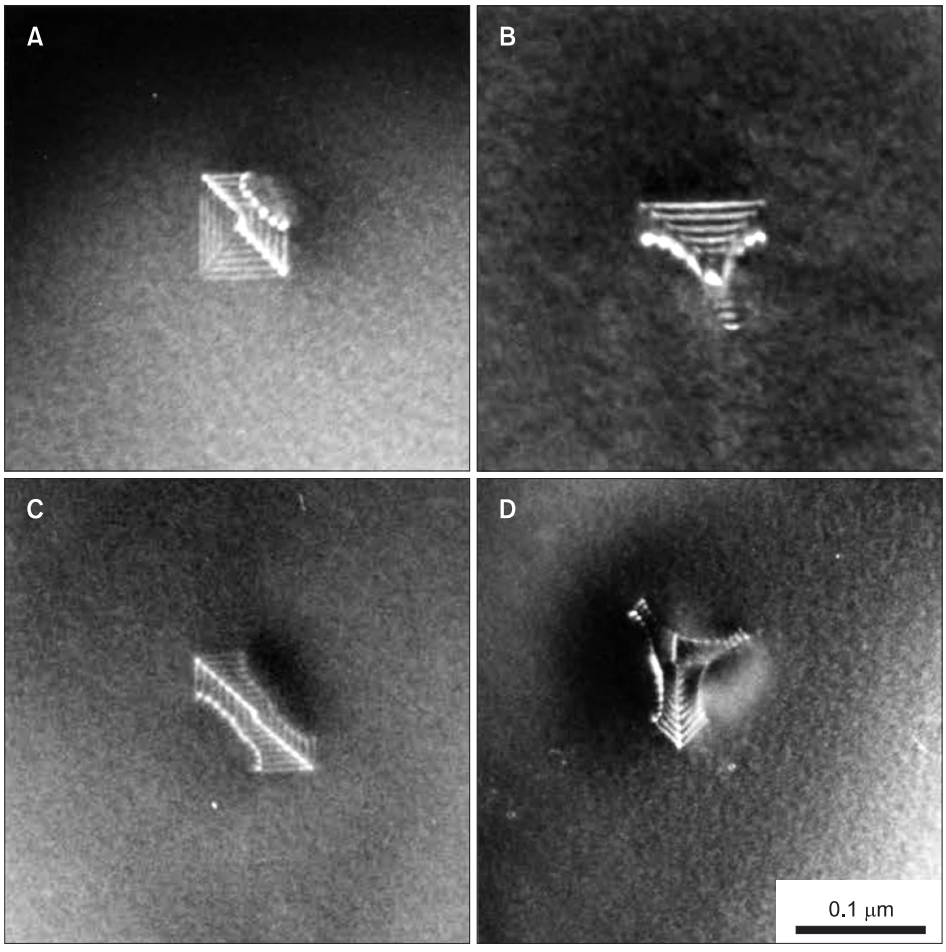

Fig. 6. Plan-view TEM micrographs of various types of imperfect SFPs. (A) L-shape, (B) T-shape, (C) I-shape, and (D) Y-shape.

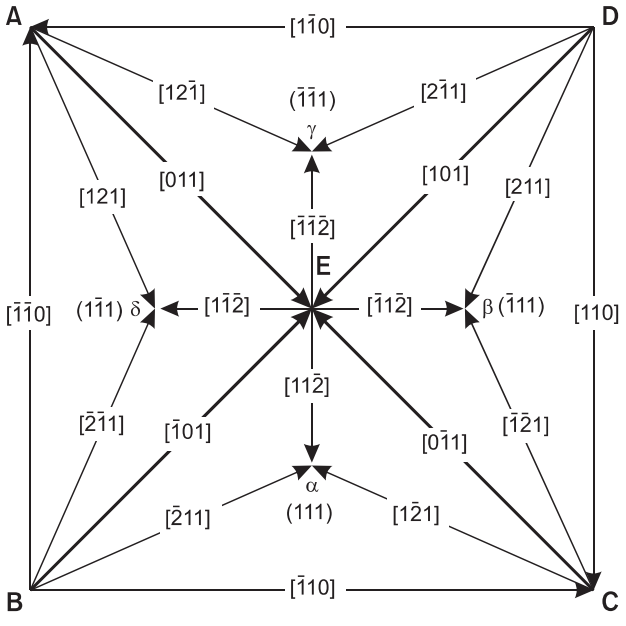

Fig. 7. Pyramidal notation along [001] direction.

question that how various shapes of SFPs are formed. Fig. 6 shows WBDF images of the four types of imperfect SFPs: 1) L-shape, 2) T-shape, 3) I-shape, and 4) Y-shape. To understand the formation of these various imperfect SFPs, we examined the stair-rod reactions obtained from various configurations of Shockley partial dislocations on each of the {111} planes. Fig. 7 shows the planar view along [001] direction of a pyramid, which is originated from half octahedron in face centered cubic structure. This pyramid consists of four {111} planes, eight [110] edges and three Shockley partials per each plane. The capital letters A, B, C, D and E denote corners of a pyramid and α, β, γ, and δ represent just midpoints of {111} planes. Notice that these notations are different to Thompson's (Hirth & Lothe, 1982; Ou et al., 2009). According to our pyramid notation the possible combination of two Shockley partials, Bα(1/6[-211]) on (111) and Eδ(1/6[1-1-2]) on (1-11), meet at the edge, BE, stair-rod dislocation BE/αβ(1/6[-101]) is formed at the [-101] edge. Possible stair-rod dislocations obtained from every combination of two Shockley partials are summarized in Table 1. There are eight kinds of stair-rod reactions, and only the (1), (2), (3), and (4) stair-rod reactions are energetically favorable but the reactions

Table 1. Possible dislocation reactions between Shockley partials

Shockley reactants $b_1 + b_2$	Stair-rod product b_3		$b_1^2 + b_2^2$ ($\times 36/a_o^2$)	b_3^2 ($\times 36/a_o^2$)
(1) Bα + Eδ	BE/αδ	1/6<110>	12	2
(2) Bα + δB	Bδ/αB	1/3<100>	12	4
(3) Bα + Dβ	BD/αβ	1/3<110>	12	8
(4) Bα + δA	Bδ/αA	1/6<310>	12	10
(5) Bα + Aδ	BA/αδ	1/6<321>	12	14
(6) Bα + βD	Bβ/αD	1/3<200>	12	16
(7) Bα + Bδ	BB/αδ	1/3<210>	12	20
(8) Bα + δE	Bδ/αE	1/6<332>	12	22

(5), (6), (7) and (8) are not. The rough excess energies can be estimated by subtracting the final energy from the initial energy of dislocations. We can see that the excess energies depend on sorts of the stair-rod dislocations and the largest excess energy is produced from the reaction (1). As the stair-rod dislocation reaction continues, the stacking fault area also expands by consuming further excess energy.

To deeply investigate the relationship between the excess energy and the energy to expand stacking fault, the critical lengths for various stair-rod dislocations were evaluated numerically. It is assumed for the calculation that the initial configuration consists of two Shockley partials (one in screw orientation and the other in 60° orientation) on adjacent {111} planes and one NSF area between the two Shockley partials with each of projected length (l) and width (w)=6.0 nm. The final configuration consists of one resulting stair-rod dislocation and the stacking fault area expanded by excess energy. Burgers vector of Shockley partials and stair-rod dislocations is b_1 and b_2, respectively. The excess energy liberated from the reaction can be calculated by using the following equation:

$$E_{XS} = E_{Sp} - E_{sr} = \left(\frac{2-1.25\nu}{1-\nu}\right)\frac{Gb_1^2\sqrt{3}l}{4\pi}\cdot\ln\left(\frac{\sqrt{3}l}{r_1}\right) - \frac{2lGb_2^2}{4\pi(1-\nu)}\cdot\ln\left(\frac{2l}{r_2}\right) \quad (1)$$

where G=5.1×10^{11} dyne/cm^2 is the shear modu1us, ν=0.28 is Poisson's ratio, γ=60 ergs/cm^2 is the intrinsic stacking fault energy. We have taken the cutoff parameters as r_1=b_1/4 and r_2=b_2/4. And the energy to expand a stacking fault can be written as:

Table 2. Excess energies and critical lengths for various stair-rod dislocations

	1/6<110>	1/3<100>	1/3<110>	1/6<310>
Excess energy ($\times 36/a_o^2$)	10	8	4	2
Critical length (nm)	90	64	20	4

$$E_{SF} = \sqrt{3}l^2\gamma - \sqrt{3}lw\gamma \quad (2)$$

where γ=60 ergs/cm^2 is the intrinsic stacking fault energy. The dislocation reaction will stop when E_{SF} is equal to E_{XS}, due to the shortage of the excess energy needed to expand further the stacking fault area. The critical length ($2l$) to form stair-rod dislocation for each reaction can be determined by using equation (1) and (2). The calculated critical length of the stair rod dislocations are listed in Table 2. The critical length of stair-rod dislocation increases as the excess energy increases. For a 1/6<110> and 1/3<100> configuration, the critical lengths are >640 Å and for a 1/3<110> and 1/6<310> configuration it is <200 Å. If the initial configuration of Shockley partials result in forming a 1/6<110> or a 1/3<100> type of stair-rod dislocation at each edge of the pyramid, a perfect SFP can be formed. However, if a 1/3<110> or a 1/6<310> type of stair-rod dislocation forms at an edge, the excess energy liberated by the reaction may expand the stacking fault on the adjacent two {111} planes incompletely and then create an imperfect SFP. Therefore, the type of stair-rod dislocation can also influence the shape of SFP.

CONCLUSIONS

SFPs at a density of 10^6 cm^{-2} are confined to the buried oxide interface. The precursors of perfect SFPs are residual precipitates pinning four dissociated dislocations (PDCs), developed by the synergistic interaction between defects and precipitates. When four NSFs react each other, resulting in four stair-rod dislocations, at each edge of a pyramid and the length of a collection of NSFs is below 620 Å, the transformation from NSFs to perfect SFP will be energetically favorable. The shape of imperfect SFPs mainly depends on the number of dissociated dislocations bounded to the top of the pyramid and the configuration of Shockley partial dislocations on the {111} pyramidal planes.

REFERENCES

Cheek T F and Chen D (1988) Dislocation reduction on SIMOX substrates by using multiple implants. *MRS Proceedings* **107**, 53.

Crean G M, Lyncrt S, Greef R, Stoemenos J, Rossow U, and Richter W (1992) Feasibility of SIMOX material quality determination using spectroellipsometry: comparison with Raman and planar view transmission electron microscopy. *MRS Proceedings* **235**, 139.

El-Ghor M K, Pennycook S J, Namavar F, and Karam N H (1990) Formation of low dislocation density silicon-on-insulator by a single implantation and annealing. *Appl. Phy. Lett.* **57**, 156.

Hill D, Fraudorf P, and Fraudorf G (1988) The reduction of dislocations in oxygen implanted silicon-on-insulator layers by sequential implantation and annealing. *J. Appl. Phys.* **63**, 4922.

Hirth J P and Lothe J (1982) *Theory of Dislocations* (Wiley, New York).

Lee J D, Park J C, Venables D, Krause S J, and Roitman P (1993) Stacking fault pyramid formation and energetics in silicon-on-insulator material formed by multiple cycles of oxygen implantation and annealing. *Appl. Phys. Lett.* **63**, 3330.

Margail J, Stoemenos J, Jaussaud C, and Bruel M (1989) Reduced defect density in silicon-on-insulator structures formed by oxygen implantation in two steps. *Appl. Phys. Lett.* **54**, 526.

Ou X, Kogler R, Skorupa W, Moller W, Wang X, and Gerlach J W (2009) Gettering layer for oxygen accumulation in the initial stage of SIMOX processing. *Nucl. Instr. Meth. B* **267**, 1273–1276.

Sears K, Wong-Leung J, Tan H H, and Jagadish C (2006) A transmission electron microscopy study of defects formed through the capping layer of self-assembled InAs/GaAs quantum dot samples. *J. Appl. Phys.* **99**, 113503.

Park J C, Lee J D, Venables D, Krause S, and Roitman P (1992) Role of oxygen precipitation processes in defect formation and evolution in oxygen implanted silicon-on-insulator material. *MRS Proceedings* **279**, 153.

van Ommen A H (1988) Low dislocation SOI by oxygen implantation. *MRS Proceedings* **107**, 43.

Venables D, Jones K S, and Namavar F (1992) Low-dislocation-density silicon-on-insulator material produced by sequential oxygen implantation and low-temperature annealing. *Appl. Phys. Lett.* **60**, 3147.